Niemi, Jonne; Balint, Roland; Engblom, Markus; Lehmusto, Juho; Lindberg, Daniel

Temperature-Gradient-Driven Aging Mechanisms in Alkali-Bromide- and Sulfate-Containing Ash Deposits

Published in:
Energy and Fuels

DOI:
10.1021/acs.energyfuels.8b04199

Published: 01/07/2019

Document Version
Publisher's PDF, also known as Version of record

energy&fuels

Article

Cite This: Energy Fuels XXXX, XXX, XXX−XXX

pubs.acs.org/EF

Temperature-Gradient-Driven Aging Mechanisms in Alkali-Bromide- and Sulfate-Containing Ash Deposits

Jonne Niemi,*[,†] Roland Balint,[†,‡] Markus Engblom,[†] Juho Lehmusto,[†] and Daniel Lindberg[†,§]

[†]Johan Gadolin Process Chemistry Centre, Laboratory of Inorganic Chemistry, Åbo Akademi University, Piispankatu 8, FI-20500 Turku, Finland

[‡]Department of Mechanical Engineering, Institute for Energy Systems, TU München, Boltzmannstraße 15, 85747 Garching, Germany

[§]Department of Chemical and Metallurgical Engineering, School of Chemical Engineering, Aalto University, Kemistintie 1, FI-00076 Aalto, Finland

ABSTRACT: The aging of alkali-bromide-containing ash deposits was studied by applying premixed alkali bromide−alkali sulfate mixtures on a laboratory-scale temperature gradient probe. The probe temperature was kept at 500 °C, while the furnace air temperature was measured to be 800 °C, simulating a heat exchanger ash deposit temperature profile. Deposits of ∼5 mm thick were aged in the furnace for 2−8 h and subsequently rapidly cooled to room temperature. The deposit cross-sections were analyzed and characterized using SEM/EDX. The deposits were observed to form multilayered structures, where the furnace-facing region was dense and sintered, while the steel-facing region was porous. Within the porous region, a gas phase migration of alkali bromides toward the colder temperature was observed. The alkali bromide migration toward the colder steel temperature observed in the experiments was quantified and compared to modeling results. The modeling results were calculated by modifying an existing temperature-gradient-driven alkali chloride intradeposit migration model for alkali bromides. The model is in agreement with the experimental results, validating an enrichment mechanism for alkali bromides. Because of their relatively high saturation pressures, alkali bromide migration was observed to be significantly faster than the earlier reported migration of alkali chlorides. Enrichment of alkali bromides in colder temperatures in boiler deposits could lead to significant changes in the local composition of the deposit, possibly leading to an enhanced corrosion rate of the tube material and/or densification of the deposit structure.

1. INTRODUCTION

Waste-derived fuels and cheap biomass fuels have become increasingly interesting for energy conversion applications. Waste-derived fuels are cheap compared to pristine biomass, and firing waste is a good alternative to landfilling.[1] Although waste firing is a lucrative alternative from the economic and environmental point of view, there exist a number of technical challenges associated with waste-derived fuels. Especially when trying to attain higher electrical efficiency by raising the final steam temperature, and as a result, the superheater material temperature, corrosion-related challenges in the boiler increase.[2]

One major challenge is the heterogeneity of the waste-derived fuels. Different waste fractions have different chemical compositions, particle sizes, etc., and the estimation of the ash chemistry and its effects on boiler design and operation is challenging. Waste fractions can include high amounts of alkali metals (Na, K), heavy metals (Pb, Zn), and halides (Cl, Br), all of which are often connected to rapid corrosion of boiler materials.[3−9] Alkali-chloride-induced high-temperature corrosion has been studied extensively, and it is recognized as one of the prominent reasons for corrosion in biomass-fired boilers. However, the detailed corrosion mechanisms are still being discussed.[2] Heavy metals in combination with Cl have also been studied to some extent, and several studies discussing the corrosion effects and mechanisms have been published.[3,4,8−11] The existing corrosion results with alkali bromides are similar to those with alkali chlorides. While high-temperature corrosion of alkali bromides has been considered in the literature,[6,7] the research on the topic is still scarce. To the best of our knowledge, alkali bromide corrosion has not been studied in the presence of a temperature gradient across the ash deposit.

One of the main sources of Br in waste-derived fuels is brominated flame-retardants, which can be found, e.g., in municipal solid waste and solid recovered fuel. Plastics treated with brominated flame-retardants can contain several mass percent Br. Brominated biocides are another important source of Br in waste-derived fuels.[12] In addition to waste, even some biomass fractions can include high amounts of Br. Naturally occurring Br mainly originates from seawater; therefore, the biomass fractions containing the most amounts of Br are some selected marine algae and coastal peat.[13]

The amount of Br in the fuel is often relatively low, e.g., in comparison to the amount of Cl. In spite of the low concentrations in the fuel, Br has been observed in the corrosion front of waterwall tubes in a BFB boiler firing a

Special Issue: 27th International Conference on Impact of Fuel Quality on Power Production and Environment

Received: December 3, 2018
Revised: February 21, 2019
Published: March 11, 2019

mixture of bark, solid recovered fuel, and wastewater sludge from a paper mill.[14] In addition, Br has been observed to enrich in waterwall deposits. Vainikka et al.[15] observed several mass percent of Br locally in waterwall deposits, while the fuel fed into the boiler contained only tens of mg kg^{-1} of Br.

Ash deposits and heat exchanger tubes experience temperature gradients during boiler operation. The temperature difference from the flue gas to the process steam/water is several hundreds of °C. Temperature gradients are known to affect the deposition behavior.[16] In addition, temperature gradients have been shown to affect corrosion of steel and the chemistry and morphology of ash deposits. Corrosion rates of the heat exchanger tube have been shown to increase with higher flue gas temperature even if the tube temperature is kept constant.[17,18] Temperature gradients have been shown to induce diffusion within oxide layers[19] and to induce penetration of corrosive chloride species through unstable oxide layers to the unaffected steel surface.[20]

The effects of temperature gradients on ash deposit chemistry and morphology have been studied mainly in laboratory scale. The main observations have so far been the formation of distinct regions within the deposit, distinguishable by either composition or structure, and migration of species due to temperature gradients.[10,21−24] Depending on the deposit composition, temperature gradients have been observed to affect the adhesion of deposits to the tube material.[25] The effect on adhesion was concluded to be mainly due to the formation of a melt, subsequent liquid phase sintering, and melt movement toward the steel surface, where it glues the deposit to the tube surface.

The temperature-gradient-induced gas phase migration of alkali chlorides has been reported and modeled earlier.[22,23] As a result of the migration, an enrichment of alkali chlorides is observed in the lower temperatures within the deposit. The alkali chlorides form pure cubical structures within the deposits and even enrich on the steel surface as pure alkali chloride crystals. Similar results have been observed in biomass-fired boilers,[26−28] and the effect has been suggested to be due to the intradeposit gas phase migration of alkali chlorides.[29]

Alkali chlorides and bromides are similar in their molecular structure, melting characteristics, and chemistry. The similarities make bromides interesting from another point of view; i.e., alkali bromides can be used to test vaporization−condensation mechanisms observed with alkali chlorides. Alkali bromides can be utilized to find out whether the phenomena, e.g., the temperature-gradient-induced alkali chloride migration, are alkali-chloride-specific or more general in nature. This paper focuses on studying the effects of temperature gradient on alkali bromide and alkali sulfate mixtures. The aim of this paper is to recognize fundamental phenomena prevailing in synthetic ash deposits, and to test the hypothesis that alkali bromide−alkali sulfate mixtures behave in a similar fashion as alkali chloride−alkali sulfate mixtures when exposed to temperature gradients. In addition, the aim is to modify and test the applicability of an existing alkali chloride migration model for alkali bromides, to further validate the understanding of the enrichment phenomena and its implications for boiler applications.

2. EXPERIMENTAL SECTION

The main experimental setup consists of a laboratory-scale air-cooled probe, which is inserted into a tube furnace. Synthetic ash deposits are applied on top of the probe. The furnace temperature is higher than the probe temperature, creating a temperature gradient over the deposit. The temperature gradient simulates a real boiler situation where a temperature gradient is present over the deposit, from the flue gas to the steam. A detailed description of the setup can be found in Lindberg et al.[22] and Niemi et al.[23]

Binary mixtures of NaBr−Na_2SO_4 and KBr−K_2SO_4 were studied in this paper. The compositions were chosen so that the melt formed at the first melting temperature is ∼60 wt % of the total mass and that the remaining solid phase is either Na_2SO_4 or K_2SO_4. The compositions of the deposit materials are shown in Table 1, together with their calculated and measured characteristic melting temperatures. Factsage thermodynamics software[30] was used to calculate the melting behavior and vapor pressure of the volatile species. The FTsalt database is one of the largest thermodynamic databases for higher-order nonideal salt systems, and contains the nonideal interaction parameters for binary (e.g., NaCl−KCl), common-ion ternary (e.g., NaCl−KCl−$ZnCl_2$), and reciprocal ternary salt systems (e.g., NaCl−KCl−Na_2SO_4−K_2SO_4). However, the thermodynamic interaction parameters for the NaBr−Na_2SO_4 and KBr−K_2SO_4 systems have not been published previously and are not included in the FTSalt database. However, the phase equilibria of NaBr−Na_2SO_4 and KBr−K_2SO_4 have been studied experimentally by Rea,[31] Palkin et al.,[32] Gromakov,[33] Flood et al.,[34] and Nyankovskaya.[35] The two binary systems are simple eutectic systems, similar to the corresponding NaCl−Na_2SO_4 and KCl−K_2SO_4 systems. On the basis of the experimental studies, the nonideal binary interaction parameters for the liquid phase were optimized using the same liquid phase solution model, the modified quasichemical model in the quadruplet approximation,[36] as Lindberg et al.[37] used for the multicomponent NaCl−Na_2SO_4−Na_2CO_3−KCl−K_2SO_4−K_2CO_3 system. The details of the assessed thermodynamic parameters will be published in a separate publication. The calculated binary phase diagrams together with experimental data are shown in Figure 1.

Table 1. Deposit Compositions and Their Calculated and Measured (in Parentheses) Characteristic Melting Temperatures, as Well as Premelt Temperatures

deposit composition [wt %]				temperature [°C]		
NaBr	Na_2SO_4	KBr	K_2SO_4	solidus	liquidus	premelt
31.5	68.5			622 (617)	719 (n.a.[a])	850
		40.6	59.4	670 (668)	845 (n.a.)	950

[a]n.a.: not available.

In addition, the melting behavior of the mixtures was studied with DSC/TGA (differential scanning calorimetry/thermogravimetric analysis), conducted with a TA Instruments SDT Q600 device. The mixtures were heated above the solidus temperature and cooled down in multiple cycles. Heating and cooling rates of 20 °C min^{-1} and a gas flow of 100 mL min^{-1} of N_2 were applied. The solidus temperatures for the mixtures were extracted from the data. The liquidus temperatures were not extracted as the vaporization of alkali bromides was kept at a minimum.

For the deposit preparation, the salt components were mixed, melted together for 20 min, quenched to room temperature, ground, and sieved to the desired size fraction (53−250 μm). The mixture preparation was conducted to obtain homogeneous salt mixtures.

The deposits were applied on the probe. The applied deposit thickness was approximately 5 mm, postexposure. The probe was inserted into a furnace where it was heated up. Once the probe reached the designated steel temperature (500 °C), cooling was initiated, and the experiment was considered to start. The furnace temperature was raised to the target temperature, which was set to 980 °C and measured ∼800 °C above the deposit. The deposits were aged in the furnace for 2, 4 or 8 h, and subsequently rapidly cooled to room temperature. The solidified deposits, together with the steel sample rings, were cast in epoxy resin, cut for a cross-section, and

DOI: 10.1021/acs.energyfuels.8b04199
Energy Fuels XXXX, XXX, XXX−XXX

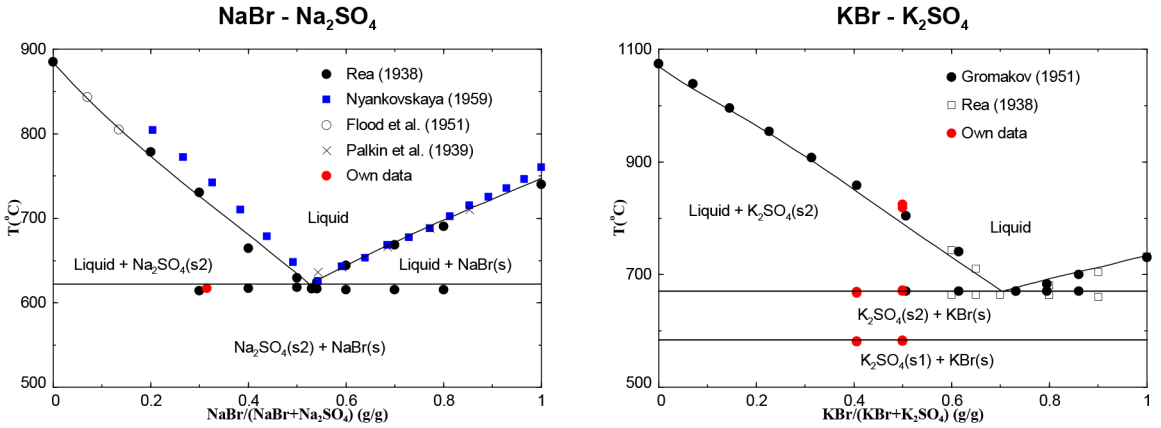

Figure 1. Calculated phase diagrams of NaBr−Na_2SO_4 and KBr−K_2SO_4 on mass basis together with the experimental data of the systems.

Table 2. Standard Chemical Compositions of EN10216-2, 10CrMo9-10, and P235GH Steels in wt %: The Rest Is Fe

steel	C	Si	Mn	P	S	Cr	Mo	N	Cu	Cr + Cu + Mo + Ni
10CrMo9-10	0.08−0.14	≤0.5	0.4−0.8	≤0.02	≤0.01	2.0−2.5	0.9−1.1	≤0.012	≤0.3	
P235GH	≤0.16	≤0.35	≤1.20	≤0.025	≤0.010					≤0.70

analyzed using SEM/EDX. All of the experiments were conducted in ambient air.

The probe houses two steel sample rings, which were both covered with the same deposit material in a given experiment, but two different steel materials were used. A low-alloyed 10CrMo9-10 steel was used as the temperature control ring (Ring 1), and a P235GH carbon steel ring was used as the temperature measurement ring (Ring 2). The standard steel compositions are shown in Table 2. The temperature control and measurement were conducted using thermocouples housed within the rings. Because of the nonuniform temperature across the probe, the measured temperature was always slightly higher than the controlled temperature. The experimental matrix is shown in Table 3.

Table 3. Experimental Matrix Showing the Steel Ring Temperatures during Experiments, with Distinct Deposit Materials and Exposure Times

temperature [°C]			
Ring 1, 10CrMo9-10	Ring 2, P235GH	deposit material	exposure time [h]
500	507	NaBr−Na_2SO_4	2
500	505	NaBr−Na_2SO_4	4
500	506	NaBr−Na_2SO_4	8
500	523	KBr−K_2SO_4	2
500	504	KBr−K_2SO_4	4
500	506	KBr−K_2SO_4	8

3. RESULTS

3.1. Above the First Melting Temperature. The SEM/EDX results for all of the experiments show a multilayered deposit morphology (Figure 2). The uppermost layer is dense and enriched in alkali sulfates. The next layer consists mainly of a mixture of alkali bromides and alkali sulfates in a ratio that is close to the eutectic composition of a NaBr−Na_2SO_4 or KBr−K_2SO_4 mixture, i.e., enriched in alkali bromides in comparison to the original composition. The eutectic composition surrounds alkali sulfate crystals (see Figure 3). Close to the steel, there is a porous region, in which the particles display similar structure to the original deposit particles; i.e., the particles do not show signs of melting during the experiment. The deposit morphology is similar to the deposit morphologies observed by Lindberg et al.[22] and Niemi et al.[23] with mixtures of alkali chlorides and alkali sulfates.

The structure of the deposits was observed to evolve as a function of time. The 2 h experiments showed, in general, more alkali bromides in the uppermost region. The amount of alkali bromides in the uppermost region decreased in 4 and 8 h experiments (Figure 3). In general, already the 2 h experiments displayed a dense upper layer, indicating that the densification occurs within a short time span.

The overall deposit structure was concluded to be similar to that observed in the alkali chloride−alkali sulfate systems, suggesting that the mechanisms responsible for the deposit structure are similar. Above the first melting temperature, the deposit aging mechanism with binary eutectic systems has been concluded to be mainly due to liquid phase sintering and temperature gradient zone melting (TGZM) phenomena.[23,24] The liquid phase sintering is supported by the fast sintering and by the holes observed in the dense deposit structure. The holes are characteristic for structures affected by liquid phase sintering occurring by the pore filling mechanism.[38]

TGZM[39] was observed to occur in all of the experiments. A distinctive feature for the mechanism is the sharp interphase between the primary crystallizing phase (alkali sulfate) and the eutectic region, mixed with alkali bromides and sulfates (see Figures 2 and 3). The pockets containing a mixture of alkali bromides and sulfates within the dense alkali sulfate structure further indicate TGZM. The phenomenon is described schematically in Figure 4. The liquid phase composition of a binary mixture, with a eutectic melting behavior, e.g., NaBr−Na_2SO_4 or KBr−K_2SO_4, depends on the temperature. In the case of NaBr−Na_2SO_4 and KBr−K_2SO_4, when the temperature of the system is between the solidus temperature and the liquidus temperature, the system will form a two-phase system. The two phases are the primary crystallizing phase, which in this case is the alkali sulfate phase, and a melt phase, which has a composition following the liquidus line of the phase diagram according to the lever rule (see Figure 4, step 2). All of the

DOI: 10.1021/acs.energyfuels.8b04199
Energy Fuels XXXX, XXX, XXX−XXX

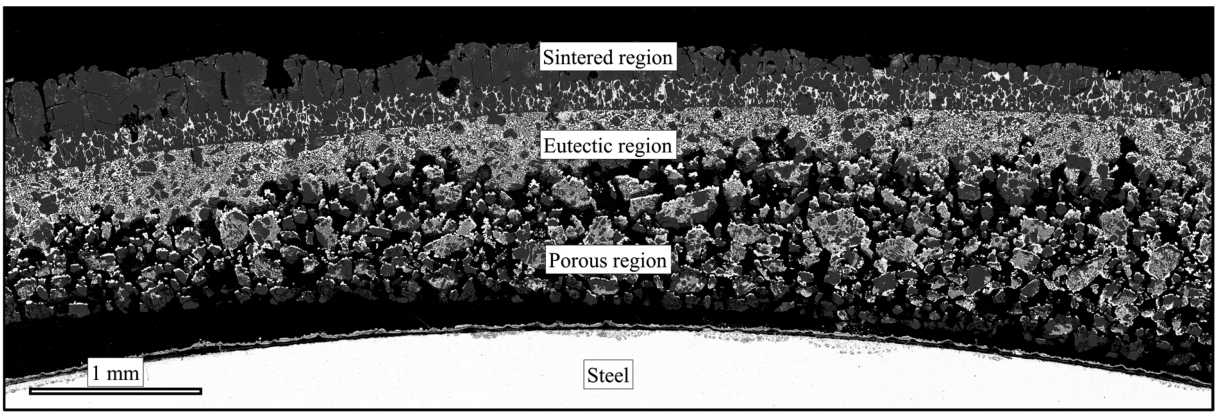

Figure 2. SEM backscatter image of the overall deposit structure of the NaBr–Na_2SO_4 deposit after 4 h of exposure. The image shows the porous, eutectic, and sintered regions. The light, dark gray, and black shades represent NaBr, Na_2SO_4, and epoxy, respectively.

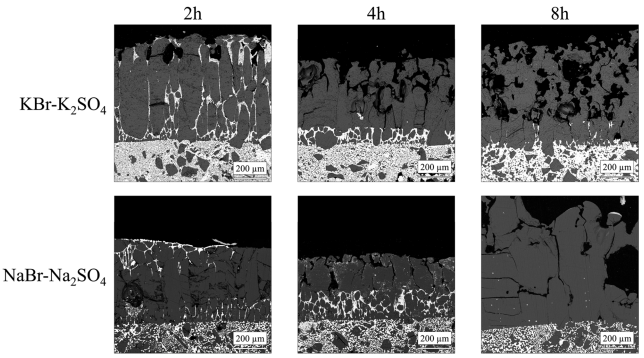

Figure 3. Evolution of the uppermost layer in the K system and in the Na system. The light, dark gray, and black shades represent (Na/K)Br, $(Na/K)_2SO_4$, and epoxy, respectively.

alkali bromide in that temperature region will be included in the melt phase.

When subjected to a temperature gradient, the melt composition differs between temperatures, creating a concentration gradient across the melt. The concentration gradient induces diffusion within the melt to balance the concentration difference. As a result, the alkali bromide migrates toward the hotter temperature; subsequently, at the lower temperature, the alkali sulfate crystallizes from the melt. The increased concentration of the alkali bromide at the higher temperature enables that more of the alkali sulfate is being incorporated into the melt phase, resulting in a bulk movement of the melt, and alkali bromide, toward the hotter temperature. At the top of the deposit, the alkali bromides vaporize into the furnace and leave behind a refined alkali sulfate structure.

In addition to the movement of alkali bromides, TGZM was observed to affect also the corrosion products. In the 8 h experiments, the upper part of the deposit cross-section and the top of the deposit were observed to have a red hue. The SEM/EDX results showed a presence of Fe within the upper part of the deposit and on the outer edge (facing the furnace air). The results from the outer edge of the 8 h experiment with 10CrMo9-10 exposed to the Na mixture are shown in Figure 5. In addition, some Fe was observed in the lower part

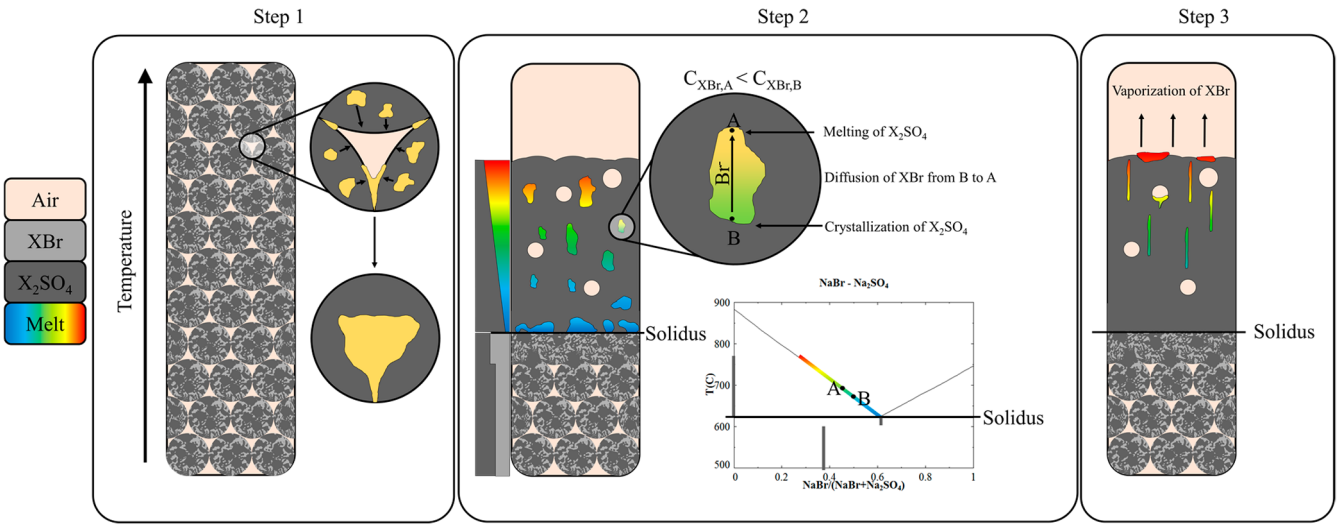

Figure 4. Schematic image explaining the deposit morphology and chemistry evolution due to liquid phase sintering and temperature gradient zone melting (TGZM) phenomena. Step 1 shows the initial deposit densification by liquid phase sintering. Step 2 shows how the TGZM induces alkali bromide migration toward the outer surface of the deposit. Step 3 shows a refined alkali sulfate structure and the sharp interface between the eutectic layer and the refined alkali sulfate.

DOI: 10.1021/acs.energyfuels.8b04199
Energy Fuels XXXX, XXX, XXX–XXX

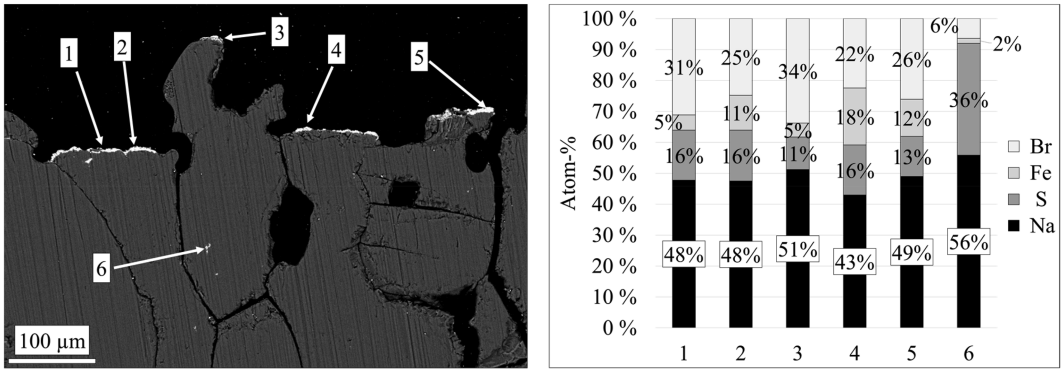

Figure 5. SEM backscatter image showing the corrosion products in the upper part of the deposit in an 8 h experiment with 10CrMo9-10 steel exposed to the NaBr−Na_2SO_4 mixture. The oxygen and carbon results are excluded from the data, because these elements are present in the epoxy.

of the eutectic layer in the 4 h experiments with P235GH steel exposed to the NaBr−Na_2SO_4 deposit. A similar behavior has been observed with alkali chloride and alkali sulfate mixtures.[21,40] However, the behavior has not been observed with alkali bromide−alkali sulfate mixtures before.

The migration of corrosion products due to TGZM is more complicated compared to the relatively simple binary mixtures (NaBr−Na_2SO_4 and KBr−K_2SO_4). With binary mixtures, the roles of the liquid phase and the primary crystallizing phase are clear, and the concentration gradient within the liquid phase is easy to concern from the phase diagram. With the inclusion of corrosion products (e.g., $FeBr_2$, $FeBr_3$, $CrBr_3$, and metal oxides), the melting properties and, consequently, the prediction of the TGMZ phenomenon become more complicated. In addition, the corrosion products are prone to oxidation with high enough O_2 partial pressures, which alters the composition and makes the system even more complicated.

Although detailed predictions of migration of corrosion products due to TGZM remain an unresolved issue and lie outside of the scope of this study, the mechanism is a plausible cause for the Fe presence at the top of the deposits exposed to temperature gradients.

3.2. Below the First Melting Temperature. Below the first melting temperature, pure alkali bromide layers were observed on the furnace-facing side of particles and on the oxide layer. In addition, on the steel-facing side of the particles, alkali-bromide-depleted areas were observed. An example of a pure alkali bromide layer and an alkali-bromide-depleted area is shown in Figure 6.

The phenomenon has been studied earlier with alkali chlorides, and it is caused by Fickian diffusion that occurs because of a temperature-gradient-induced concentration gradient in the gas phase.[22,23] Alkali bromides vaporize from the steel-facing side of the particle, leaving behind an alkali sulfate scaffold. The vaporized alkali bromides migrate toward the colder temperature, i.e., toward the steel surface. Subsequently, the alkali bromides condense on a colder surface because of supersaturation in the gas phase. The colder surface can be either the furnace-facing side of an ash particle below the particle of origin, or the steel surface. The vaporization−condensation mechanism results in a bulk migration of alkali bromides toward the colder temperature, i.e., toward the steel surface.

The alkali bromide migration layer thicknesses were quantified as described by Lindberg et al.,[22] and the results,

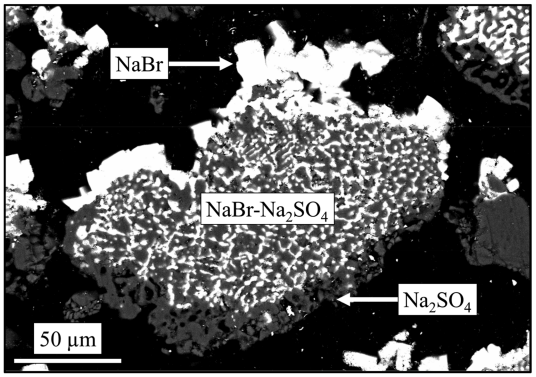

Figure 6. SEM backscatter image showing NaBr enrichment on the top of a NaBr−Na_2SO_4 particle and NaBr depletion at the bottom of the particle.

as a function of temperature, are shown in Figure 7. An existing migration model for alkali chlorides[23] was modified to predict the alkali bromide migration. The species-specific values were modified (see Table 4), and the differences in the densities of the alkali bromides and sulfates were taken into account. The values shown in Table 4 are utilized for partial pressure calculations and for diffusion coefficient estimation, according to the kinetic theory of gases.

The model describes the Fickian diffusion of volatile species due to the temperature-gradient-induced concentration gradient. The concentration gradient, and therefore the diffusion flux, is directly proportional to the temperature gradient across the gas phase. The temperature gradient across the gas phase was estimated from the bulk temperature gradient across the porous layer, and from the estimated porosity of the deposit. The temperature gradients across the porous layers in individual experiments were estimated from the SEM images. The temperature gradient (dT/dx) values were estimated to be 65−90 °C mm^{-1} for the KBr−K_2SO_4 mixtures and 70−115 °C mm^{-1} for the NaBr−Na_2SO_4 mixtures, and they are shown in Figure 7. In the model calculations, the bulk temperature gradient was multiplied by a correction factor of 3.7 to account for the steeper temperature gradient across the gas phase than across the solid phase (for additional information, see Niemi et al.[23]). In addition, the logarithm of the alkali bromide saturation pressure is linearly proportional to the inverse absolute temperature, ergo the logarithm of the concentration gradient is linearly proportional to the inverse absolute

DOI: 10.1021/acs.energyfuels.8b04199
Energy Fuels XXXX, XXX, XXX−XXX

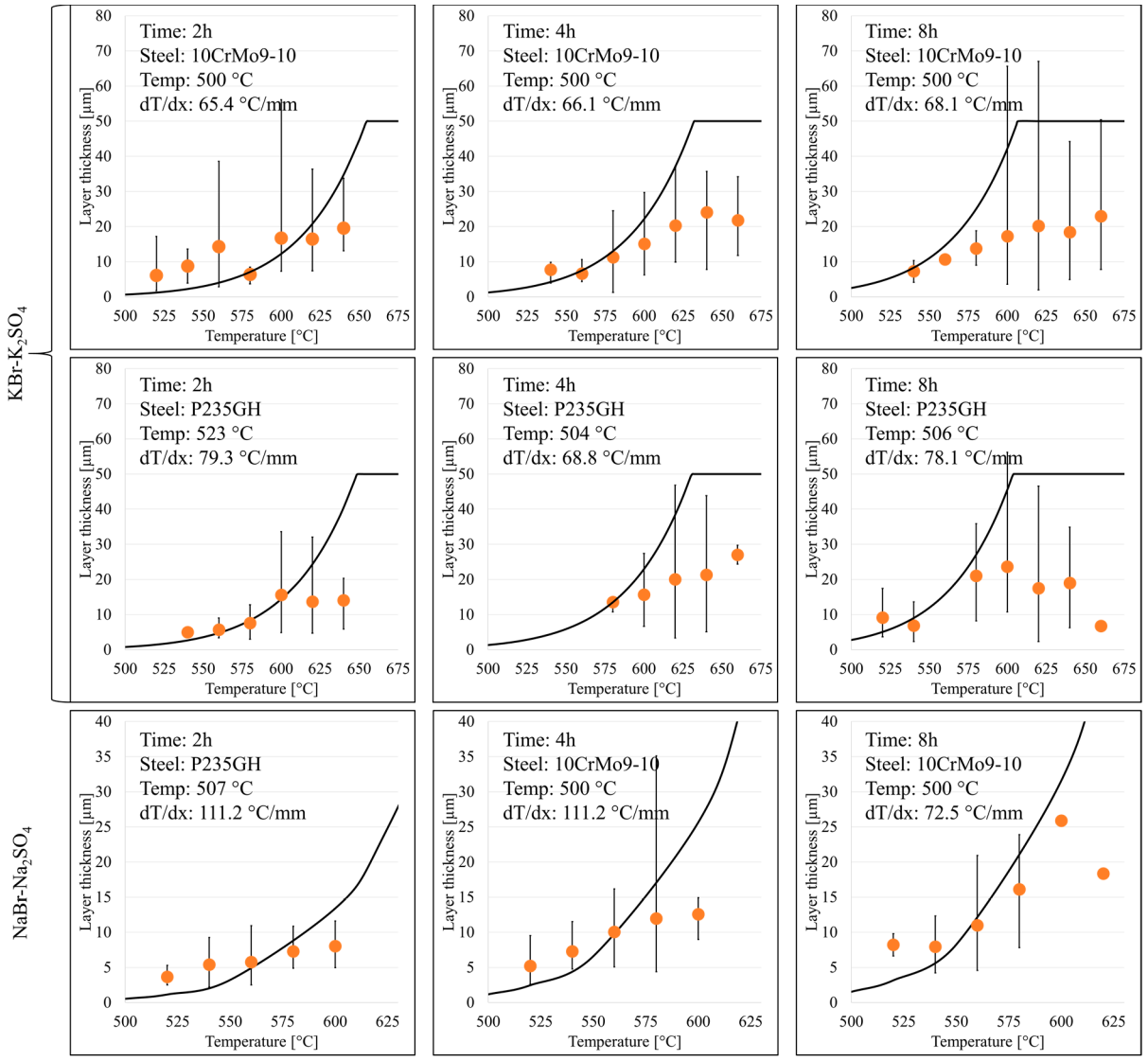

Figure 7. Average measured alkali bromide layer thicknesses (dots) together with modeled results (continuous line) as a function of temperature in individual experiments. The error bars show the maximum and minimum thickness values measured in the temperature interval (20 °C) in question.

Table 4. Molecule-Dependent Constants for Determining the Saturation Pressures (A_i and B_i) of Alkali Bromides, Effective Molecular Diameters in the N_2 Atmosphere ($d_{i,\mathrm{eff}}$), Effective Mass in the N_2 Atmosphere (μ_i), and Density at Room Temperature (ρ_i)[30,41,42]

component, i	A_i [K]	B_i [−]	$d_{i,\mathrm{eff}}$ [m]	μ_i [kg]	ρ_i [kg m^{-3}]
KBr	−24 298	16.07	3.68×10^{-10}	3.77×10^{-26}	2750
$(KBr)_2$	−27 388	18.08	4.74×10^{-10}	4.16×10^{-26}	2750
NaBr	−24 850	16.19	3.41×10^{-10}	3.66×10^{-26}	3210
$(NaBr)_2$	−26 308	17.25	4.54×10^{-10}	4.10×10^{-26}	3210

temperature, which results in an exponential increase in the diffusion flux as a function of the absolute temperature.

The model estimates a decrease in the diffusion flux as a function of time. The effective diffusion coefficient decreases, as the gaseous species need to travel longer within the particle of origin as it is depleted of the alkali bromides as a function of time. A similar decrease in the migration rate was observed also in the experimental results. The initial particle-to-particle distance in the model was chosen to be 50 μm, corresponding to the experimental observations and to the solids fraction of close-packing structures (0.74) in one dimension when a particle size of 150 μm is applied. The initial particle-to-particle distance was also used as a boundary condition for the model; i.e., the maximum alkali bromide layer thickness was limited to 50 μm. The modeled values are plotted together with the corresponding experimental results in Figure 7.

The model values agree reasonably well with the experimental values in lower temperatures and with short exposure times. The deviations in the higher temperatures and with longer exposure times are understandable as the predicted

DOI: 10.1021/acs.energyfuels.8b04199
Energy Fuels XXXX, XXX, XXX−XXX

layer thicknesses are unreasonably thick for the experimental setup, which results in pronounced deviations with longer experiments and in higher temperatures. In the experiment with KBr−K_2SO_4 on the P235GH steel with 4 h of exposure, where no layer data is reported for low temperatures, the lower temperature part of the porous layer was missing. The loss of deposit material is due to the deposit preparation in the cutting stage. The loss of deposit material after the cutting phase of the sample preparation was observed as a lack of deposit material and epoxy resin. The 2 h exposure of 10CrMo9-10, and the 4 and 8 h exposures of P235GH to NaBr−Na_2SO_4, showed a missing porous layer, which is why no layer growth data is available for those experiments.

Regardless of the deviation of the modeled values from the experimental values in the higher temperatures, the results imply that the underlying phenomenon, i.e., the temperature-gradient-induced gas phase migration, is successfully recognized for the alkali bromides. The model results are in reasonably good agreement with the experimental values, which indicates that the model can be utilized for deposit aging calculations if some limitations are considered. The limitations include space limitations for the layer growth, lower activity for the gaseous species due to solid or liquid solutions, and mass balance limitations. The results of this paper confirm the hypothesis that the temperature-gradient-induced diffusion mechanism observed with alkali chlorides also applies for other volatile compounds found in ash deposits.

Compared to alkali chlorides, the alkali bromide migration was observed to occur at a higher rate in the same temperature range and with the same temperature gradient. The calculated saturation pressure of alkali halides at a set temperature increases when the size of either the cation or the anion increases (KCl > NaCl > LiCl, NaBr > NaCl > NaF). The saturation pressure of alkali halides increases exponentially as a function of temperature. In a set temperature and temperature gradient, the partial pressure gradient is steeper for the species with the higher saturation pressure (KCl > NaCl > LiCl, NaBr > NaCl > NaF), resulting in a higher diffusion flux.

3.3. Corrosion. Significant corrosion was observed in all of the experiments. With P235GH, the corrosion layer consisted typically of alkali bromides, iron oxide, iron bromides, and a combination of all of the aforementioned. 10CrMo9-10 produced a similar oxide layer but included also Cr species. Already the 2 h experiments resulted in oxide layer thicknesses of ∼10 μm, but the oxide layer growth rate seemed to slow down rapidly after the initial oxide layer formation.

Figure 8 shows a typical corrosion layer of P235GH from the 4 h experiment, with the KBr−K_2SO_4 mixture. Just above the steel surface, Br was observed, but little to no alkali metals were observed, indicating a formation of metal bromides. A similar distribution of elements was observed also with the other experiments. With P235GH, Br was observed together with Fe, while with 10CrMo9-10, Br was observed together with Fe and Cr. $FeBr_2$, $FeBr_3$, $NiBr_2$, and $CrBr_3$ have been observed to form at steel surfaces exposed to Br_2 and high temperatures.[43]

Above the metal bromides, a dense oxide layer was observed. For P235GH, the oxide layer contained mainly iron oxides. With 10CrMo9-10, the oxide layer consisted of a mixture of iron and chromium oxides. The dense oxide layer did not contain Br with either of the tested steels and regardless of the exposure time.

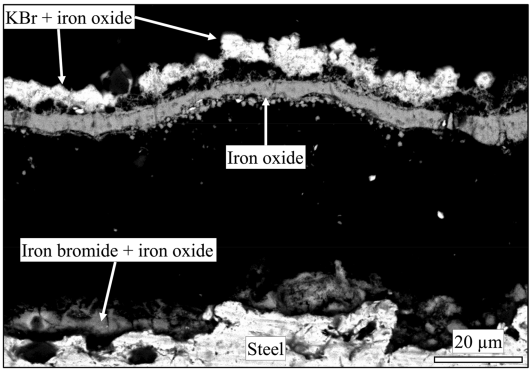

Figure 8. Corrosion layer of P235GH steel after 4 h of exposure to KBr−K_2SO_4.

On top of the dense oxide layer, pure crystals of alkali bromides were detected for all of the experiments. The crystals are a result of the vaporization−condensation of alkali bromides within the deposit. The mechanism can be clearly seen to enrich alkali bromides at the oxide layer.

In the experiment with P235GH exposed to NaBr−Na_2SO_4 for 4 h, in addition to the dense oxide layer, a more porous oxide layer was observed to grow on top of and around the salt particles near the steel surface. In addition, indications of iron bromides were observed above the dense oxide layer, close to salt particles (Figure 9). In the same experiment and in the 8 h experiment with 10CrMo9-10 steel exposed to the NaBr−Na_2SO_4 mixture, corrosion products were found in the upper parts of deposits, which indicates vaporization of corrosion products and condensation within the deposit. This occurs due to an oxygen potential gradient from the metal surface, where it is buffered by the metal−metal oxide equilibrium, to the air in the furnace. With low oxygen potential, volatile metal halide species (e.g., $FeCl_2$, $FeCl_3$, $FeBr_2$, $FeBr_3$) can vaporize close to the metal−metal oxide interface and subsequently react to metal oxides when they reach a location within the deposit with higher oxygen potential.

Similar corrosion behavior, where the oxide layer grows around the deposit salt particles, has been observed with 10CrMo9-10 steel exposed to KBr[6] and to NaCl or KCl[44] at high temperatures in isothermal conditions. Enestam et al.[44] proposed that the porous oxide layer formation in NaCl and KCl deposits is due to the formation and subsequent vaporization of metal halides, which then react to metal oxides and condense on the salt particles above the steel surface. Wu et al.[6] reported analogous behavior with KBr. To the best our knowledge this is the first study showing similar corrosion behavior of steel exposed to NaBr.

4. IMPLICATIONS

Deposit aging has direct effects on the deposit removability and chemistry. The results of Laxminarayan et al.[25] show that liquid phase sintering of deposits and liquid movement toward the steel surface increase the adhesion strength of deposits to the heat exchanger surfaces. They also note that gas phase migration of alkali chlorides plays a role in the evolution of the deposit adhesion strength. The results of this study show that even alkali bromides migrate within ash deposits and can potentially enrich on heat exchanger surfaces, affecting both corrosion and deposit adhesion strength. Already low Br

DOI: 10.1021/acs.energyfuels.8b04199
Energy Fuels XXXX, XXX, XXX−XXX

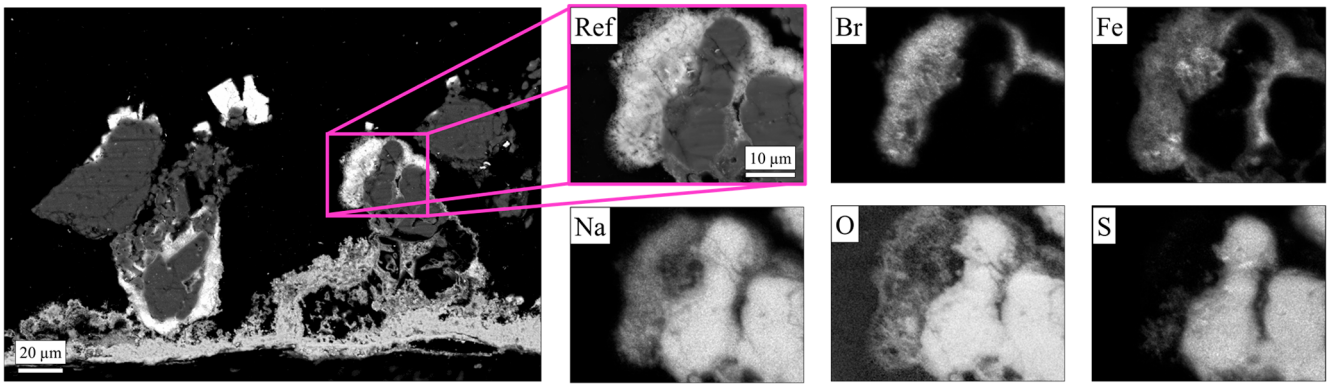

Figure 9. SEM image showing the porous oxide layer of P235GH steel after 4 h of exposure to $NaBr-Na_2SO_4$.

concentrations in the fuel have been shown to result in enrichment of Br in waterwall deposits.[15]

The results of Costa and Paoliello[45] show that the deposit composition in a black liquor recovery boiler can vary greatly from the inner to the outer part of the deposit. They observed high concentrations of K and Cl close to the steel surface, which could be due to the enrichment of K and Cl in the melt phase, which has migrated to the steel surface. Similar results have been reported by Reeve et al.[46] Although alkali bromides are not commonly found in recovery boilers, the results of this study further indicate which mechanisms are responsible for the enrichment of alkali chlorides in cold temperatures, i.e., gas phase migration and liquid phase sintering.

In the present work, migration of gaseous alkali bromides toward the colder temperatures was shown to occur due to temperature gradients. The migration rate increases as a function of both the local temperature and the temperature gradient. This implies that, in boiler design, in addition to the absolute temperature of the heat exchanger material, the temperature gradient from the flue gas to the steel also affects the corrosion risk. Others have reported results, which support this view.[17,18]

The temperature-gradient-induced gas phase migration model has been shown to qualitatively work with alkali chlorides and alkali bromides. The model relies on Fick's first law of diffusion and on the kinetic theory of gases, which makes it also easily applicable for other volatile species within deposits and for other applications where temperature gradients are present. For technically relevant detailed results, the migration model would probably need to be used in combination with thermodynamic modeling, as the partial pressures of volatile species are connected to the solid and liquid phases locally present in the deposit. In turn, the gas phase migration affects the local compositions within the deposit, resulting in a highly dynamic system, where the phase composition would need to be re-evaluated continuously.

The synthetic deposits used in this study differ from actual boiler deposits in a number of ways. The compositions of the deposits used in this study are simple binary eutectics, with relatively high alkali bromide concentration compared to boiler environments. The boiler deposit contains many different components, depending on the fuel. For biomass fuels, the main ash-forming elements are Ca, K, Si, and Mg.[47] With waste-derived fuels, the ash composition is even more complicated, and the deposit can in addition contain, e.g., high amounts of Pb and Zn.[8]

Boiler ash deposits are often heterogeneous in nature, with different compositions and structures across the deposit, mainly due to the way of the deposit formation. The deposit formation in a boiler occurs by several different mechanisms that occur simultaneously, condensation, thermophoresis, eddy impaction, and inertial impaction being the most common deposit formation mechanisms.[48] The deposit formation mechanisms, as well as the ash composition, affect the deposit structure. Deposits vary greatly in nature between boilers and locations within the boiler. Contrary to boiler deposits, the deposits used in this study are homogeneous both in composition and in structure at the beginning of the experiments. However, the synthetic deposits were observed to become increasingly heterogeneous because of the exposure to temperature gradients. This indicates that even deposit aging can contribute to the deposit structure and composition. There are indications that deposit aging also affects the local composition and structure of ash deposits.[28,29]

The vaporization−condensation mechanism of volatile species can only occur if there are volatile species present within the deposit, and the deposit structure is porous; i.e., there are void spaces available for the volatile species to condense to. Several studies have shown that boiler deposits are indeed porous;[28,49,50] however, parameters, such as the fuel, the location in the boiler, and the temperature profile, affect the porosity and the pore size. The pore size will most likely limit the migration rate of the volatile species within the deposits. The vaporization−condensation mechanism is expected to occur at a slower pace in boiler deposits than in the synthetic deposits in question. There are additional limiting factors that are present in boiler deposits; e.g., the volatile species might be part of a solid or liquid solution, which results in their lower partial pressure. In addition, the amount of the volatile species is likely to be fairly low within the deposits, which also limits the potential for enrichment in lower temperatures. However, alkali bromides have been observed to enrich at lower temperatures within deposits, i.e., close to the steel surface.[15] The enrichment is likely to be caused by both the deposit build-up mechanisms (i.e., alkali bromide condensation from the flue gas) and the deposit aging mechanisms (i.e., intradeposit vaporization−condensation and liquid phase sintering).

The liquid phase sintering and TGZM both require a melt phase present to occur. In addition, liquid phase sintering can only occur in a porous deposit, while TGZM requires a continuous solid phase in order to occur. Liquid phase sintering is likely to occur in boiler deposits, but the extent of it

DOI: 10.1021/acs.energyfuels.8b04199
Energy Fuels XXXX, XXX, XXX−XXX

is still unclear. The sintering tendency has been shown to be connected to the amount of melt present.[23] The amount of melt in a boiler deposit is likely to be significantly lower than in the synthetic ash deposits studied in this paper, which will result in lesser deposit densification. In addition, boiler deposits may contain molten phases with high viscosity, with which the sintering effects are expected to be slower. However, in boilers the deposits have a longer time to mature.

The industrial relevance of TGZM in boiler deposits remains unclear. TGZM could potentially alter the corrosion rate of heat exchanger tubes. On one hand, with optimal conditions, TGZM can induce migration of corrosive halide species toward the fuel gas, i.e., away from the steel surface. On the other hand, TGZM can induce migration of corrosion products or parts of the protective oxide layer toward the hotter temperature, resulting in an exposed steel surface and rapid corrosion.

5. CONCLUSIONS

Steel samples were covered with mixtures of alkali bromides and alkali sulfates and exposed to industrially relevant temperature gradients to study the corrosion of steel and aging mechanisms occurring in ash deposits. The results show similar behavior to alkali chloride and alkali sulfate mixtures. Both display liquid phase sintering and temperature gradient zone melting in supersolidus temperatures. In subsolidus temperatures, gas phase migration toward the colder temperatures was observed to occur for alkali bromides. An existing one-dimensional alkali chloride migration model was modified to predict the alkali bromide migration. The predicted amount of alkali bromides (layer thickness) is correctly predicted for short exposure times in low temperatures (<600 °C). The predictions deviate for longer exposure times and in locations of the deposit where the migration rate is the fastest. The most likely reason for the deviation is that the alkali bromide migration is limited in the experimental deposit by the limited void space available for layer growth. The corrosion results show the formation of metal bromides at the steel surface.

AUTHOR INFORMATION

Corresponding Author

*E-mail: joniemi@abo.fi.

ORCID

Jonne Niemi: 0000-0002-7840-7658

Notes

The authors declare no competing financial interest.

ACKNOWLEDGMENTS

This work was conducted within the Academy of Finland project "Understanding the dynamics of intradeposit chemistry and morphology for control of corrosion in high temperature processes" (Decision 310266) as part of the activities of the Johan Gadolin Process Chemistry Centre at Åbo Akademi University. Additional funding from the Graduate School in Chemical Engineering (GSCE) and from the Academy of Finland (Decisions 266384 and 296435) for three of the authors (J.N., D.L., and J.L., respectively) is greatly appreciated. The authors would like to thank Linus Silvander for operating the SEM apparatus, Peter Backman for operating the DSC/TGA apparatus, and Jaana Paananen for her help with the experimental setup and sample preparation.

REFERENCES

(1) Cucchiella, F.; D'Adamo, I.; Gastaldi, M. Sustainable waste management: Waste to energy plant as an alternative to landfill. *Energy Convers. Manage.* **2017**, *131*, 18−31.

(2) Hupa, M.; Karlström, O.; Vainio, E. Biomass combustion technology development − It is all about chemical details. *Proc. Combust. Inst.* **2017**, *36* (1), 113−134.

(3) Bankiewicz, D.; Enestam, S.; Yrjas, P.; Hupa, M. Experimental studies of Zn and Pb induced high temperature corrosion of two commercial boiler steels. *Fuel Process. Technol.* **2013**, *105*, 89−97.

(4) Kinnunen, H.; Hedman, M.; Engblom, M.; Lindberg, D.; Uusitalo, M.; Enestam, S.; Yrjas, P. The influence of flue gas temperature on lead chloride induced high temperature corrosion. *Fuel* **2017**, *196*, 241−251.

(5) Sánchez Pastén, M.; Spiegel, M. High temperature corrosion of metallic materials in simulated waste incineration environments at 300−600 °C. *Mater. Corros.* **2006**, *57* (2), 192−195.

(6) Wu, H.; Yrjas, P.; Hupa, M. Laboratory Studies of Potassium-Halide-Induced High-Temperature Corrosion of Superheater Steels. Part 1: Exposures in Dry Air. *Energy Fuels* **2015**, *29* (2), 1186−1195.

(7) Wu, H.; Bankiewicz, D.; Yrjas, P.; Hupa, M. Laboratory Studies of Potassium-Halide-Induced High-Temperature Corrosion of Superheater Steels. Part 2: Exposures in Wet Air. *Energy Fuels* **2015**, *29* (4), 2709−2718.

(8) Sorell, G. The Role of Chlorine in High Temperature Corrosion in Waste to Energy Plants. *Mater. High Temp.* **1997**, *14* (3), 207−220.

(9) Niemi, J.; Kinnunen, H.; Lindberg, D.; Enestam, S. Interactions of PbCl2 with Alkali Salts in Ash Deposits and Effects on Boiler Corrosion. *Energy Fuels* **2018**, *32* (8), 8519−8529.

(10) Kinnunen, H.; Lindberg, D.; Laurén, T.; Uusitalo, M.; Bankiewicz, D.; Enestam, S.; Yrjas, P. High-temperature corrosion due to lead chloride mixtures simulating fireside deposits in boilers firing recycled wood. *Fuel Process. Technol.* **2017**, *167*, 306−313.

(11) Enestam, S.; Backman, R.; Mäkelä, K.; Hupa, M. Evaluation of the condensation behavior of lead and zinc in BFB combustion of recovered waste wood. *Fuel Process. Technol.* **2013**, *105*, 161−169.

(12) Vainikka, P.; Hupa, M. Review on bromine in solid fuels - Part 2: Anthropogenic occurrence. *Fuel* **2012**, *94* (1), 34−51.

(13) Vainikka, P.; Hupa, M. Review on bromine in solid fuels. Part 1: Natural occurrence. *Fuel* **2012**, *95* (1), 1−14.

(14) Vainikka, P.; Enestam, S.; Silvennoinen, J.; Taipale, R.; Yrjas, P.; Frantsi, A.; Hannula, J.; Hupa, M. Bromine as an ash forming element in a fluidised bed boiler combusting solid recovered fuel. *Fuel* **2011**, *90* (3), 1101−1112.

(15) Vainikka, P.; Bankiewicz, D.; Frantsi, A.; Silvennoinen, J.; Hannula, J.; Yrjas, P.; Hupa, M. High temperature corrosion of boiler waterwalls induced by chlorides and bromides. Part 1: Occurrence of the corrosive ash forming elements in a fluidised bed boiler co-firing solid recovered fuel. *Fuel* **2011**, *90* (5), 2055−2063.

(16) Baxter, L. L. Ash Deposition during Biomass and Coal Combustion: A Mechanistic Approach. *Biomass Bioenergy* **1993**, *4* (2), 85−102.

(17) Brossard, J. M.; Diop, I.; Chaucherie, X.; Nicol, F.; Rapin, C.; Vilasi, M. Superheater fireside corrosion mechanisms in MSWI plants: Lab-scale study and on-site results. *Mater. Corros.* **2011**, *62*, 543−548.

(18) Brossard, J. M.; Lebel, F.; Rapin, C.; Mareche, J.-F.; Chaucherie, X.; Nicol, F.; Vilasi, M. Lab-scale study on fireside superheaters corrosion in MSWI plants. In *NAWTEC17*, Proceedings of the 17th annual North American waste to energy conference, Chantilly, Virginia, United States, 2009; pp 63−69.

(19) Covino, B. S., Jr.; Holcomb, G. R.; Cramer, S. D.; Bullard, S. J.; Ziomek-Moroz, M.; White, M. L. Corrosion in a temperature gradient. In *17th Annual Conference on Fossil Energy Materials 2003*.

(20) Kawahara, Y. Evaluation of high-temperature corrosion life using temperature gradient corrosion test with thermal cycle component in waste combustion environments. *Mater. Corros.* **2006**, *57*, 60−72.

DOI: 10.1021/acs.energyfuels.8b04199
Energy Fuels XXXX, XXX, XXX−XXX

(21) Lagerbom, J.; Lepistö, T.; Backman, R.; Hupa, M. Behavior of alkaline sulfate-chloride salts in temperature gradient corrosion test furnace. In *VTT Symp.*, 2001; pp 541−551.
(22) Lindberg, D.; Niemi, J.; Engblom, M.; Yrjas, P.; Lauren, T.; Hupa, M. Effect of temperature gradient on composition and morphology of synthetic chlorine-containing biomass boiler deposits. *Fuel Process. Technol.* **2016**, *141*, 285−298.
(23) Niemi, J.; Lindberg, D.; Engblom, M.; Hupa, M. Simultaneous melt and vapor induced ash deposit aging mechanisms − Mathematical model and experimental observations. *Chem. Eng. Sci.* **2017**, *173*, 196−207.
(24) Niemi, J.; Lindberg, D.; Engblom, M.; Tran, H. A Fundamental Study on the Change in Composition of Fireside Deposits with Time in Kraft Recovery Boilers. *J. Sci. Technol. For. Prod. Processes* **2018**, *7* (2), 45−52.
(25) Laxminarayan, Y.; Nair, A. B.; Jensen, P. A.; Wu, H.; Frandsen, F. J.; Sander, B.; Glarborg, P. Tensile Adhesion Strength of Biomass Ash Deposits: Effect of the Temperature Gradient and Ash Chemistry. *Energy Fuels* **2018**, *32* (4), 4432−4441.
(26) Michelsen, H. P.; Frandsen, F.; Dam-Johansen, K.; Larsen, O. H. Deposition and high temperature corrosion in a 10 MW straw fired boiler. *Fuel Process. Technol.* **1998**, *54* (1−3), 95−108.
(27) Hansen, L. A.; Nielsen, H. P.; Frandsen, F. J.; Dam-Johansen, K.; Horlyck, S.; Karlsson, A. Influence of deposit formation on corrosion at a straw-fired boiler. *Fuel Process. Technol.* **2000**, *64* (1−3), 189−209.
(28) Jensen, P. A.; Frandsen, F. J.; Hansen, J.; Dam-Johansen, K.; Henriksen, N.; Hörlyck, S. SEM investigation of superheater deposits from biomass-fired boilers. *Energy Fuels* **2004**, *18* (2), 378−384.
(29) Wu, D.; Dahl, K. V.; Madsen, J. L.; Christiansen, T. L.; Montgomery, M.; Hald, J. Effects of Different Fuel Specifications and Operation Conditions on the Performance of Coated and Uncoated Superheater Tubes in Two Different Biomass-Fired Boilers. ACS Appl. *Energy Mater.* **2018**, *1* (4), 1463−1475.
(30) Bale, C. W.; Belisle, E.; Chartrand, P.; Decterov, S. A.; Eriksson, G.; Gheribi, A. E.; Hack, K.; Jung, I. H.; Kang, Y. B.; Melancon, J.; Pelton, A. D.; Petersen, S.; Robelin, C.; Sangster, J.; Spencer, P.; Van Ende, M. A. FactSage thermochemical software and databases, 2010−2016. CALPHAD: *CALPHAD: Comput. Coupling Phase Diagrams Thermochem.* **2016**, *54*, 35−53.
(31) Rea, R. F. Temperature-measuring cones. *J. Am. Ceram. Soc.* **1938**, *21*, 98−101.
(32) Palkin, A. P.; Gromakov, S. D.; Reshetnikov, P. F.; Semenov, N. I.; Turusov, M. G. Ternary fusibility systems. *Acta Univ. Voronegiensis (U. S. S. R.)* **1939**, *10* (4), 5−39.
(33) Gromakov, S. D. Some rules pertaining to the determination of the type of phase diagrams of binary systems. *Zh. Fiz. Khim.* **1951**, *25*, 1014−1025.
(34) Flood, H.; Forland, T.; Nesland, A. Cryoscopic measurements in fused salts at elevated temperatures. *Acta Chem. Scand.* **1951**, *5*, 1193−1198.
(35) Nyankovskaya, R. N. Fusion diagram for the system of the sulfates and bromides of sodium and potassium. *Zh. Neorg. Khim.* **1959**, *4*, 2591−2595.
(36) Pelton, A. D.; Chartrand, P.; Eriksson, G. The modified quasi-chemical model: Part IV. Two-sublattice quadruplet approximation. *Metall. Mater. Trans. A* **2001**, *32* (6), 1409−1416.
(37) Lindberg, D.; Backman, R.; Chartrand, P. Thermodynamic evaluation and optimization of the (NaCl+Na2SO4+Na2CO3+KCl +K2SO4+K2CO3) system. *J. Chem. Thermodyn.* **2007**, *39* (7), 1001−1021.
(38) German, R. M.; Suri, P.; Park, S. J. Review: liquid phase sintering. *J. Mater. Sci.* **2009**, *44* (1), 1−39.
(39) Pfann, W. G. Temperature Gradient Zone Melting. *JOM* **1955**, *7* (9), 961−964.
(40) Lindberg, D.; Niemi, J.; Engblom, M.; Laurén, T.; Yrjas, P.; Hupa, M. Experimental and modeling approaches to simulate temperature-gradient induced intradeposit chemical processes with implications for biomass boiler corrosion. 23rd International Conference on FBC, Grand Ambassador Seoul, Seoul, South Korea, May 13−17, 2018; C9−1, pp 1124−1134.
(41) Shannon, R. D. Revised Effective Ionic-Radii and Systematic Studies of Interatomic Distances in Halides and Chalcogenides. *Acta Crystallogr., Sect. A: Cryst. Phys., Diffr., Theor. Gen. Crystallogr.* **1976**, *32* (SEP1), 751−767.
(42) Torring, T.; Biermann, S.; Hoeft, J.; Mawhorter, R.; Cave, R. J.; Szemenyei, C. The structure of alkali halide dimers: A critical test of ionic models and new ab initio results. *J. Chem. Phys.* **1996**, *104* (20), 8032−8042.
(43) Lee, S.; Tsujikawa, S. Corrosion behavior of Fe-Cr and Fe-Ni-base commercial alloys in flowing Ar-42.6%O-2−14.7%Br-2 gas mixture at 700 degrees C. *Mater. Corros.* **1997**, *48* (6), 364−371.
(44) Enestam, S.; Bankiewicz, D.; Tuiremo, J.; Mäkelä, K.; Hupa, M. Are NaCl and KCl equally corrosive on superheater materials of steam boilers? *Fuel* **2013**, *104*, 294−306.
(45) Costa, D. S.; Paoliello, F. A. Experience of recovery boiler superheater corrosion at Cenibra. In *International Chemical Recovery Conference*; Halifax, Nova Scotia, 2017.
(46) Reeve, D. W.; Tran, H. N.; Barham, D. Superheater Fireside Deposits and Corrosion in Kraft Recovery Boilers. *Tappi J.* **1981**, *64* (5), 109−113.
(47) Vassilev, S. V.; Baxter, D.; Andersen, L. K.; Vassileva, C. G. An overview of the chemical composition of biomass. *Fuel* **2010**, *89* (5), 913−933.
(48) Kleinhans, U.; Wieland, C.; Frandsen, F. J.; Spliethoff, H. Ash formation and deposition in coal and biomass fired combustion systems: Progress and challenges in the field of ash particle sticking and rebound behavior. *Prog. Energy Combust. Sci.* **2018**, *68*, 65−168.
(49) Zhou, H.; Zhou, B.; Zhang, H.; Li, L.; Cen, K. Investigation of Slagging Characteristics in a 300 kW Test Furnace: Effect of Deposition Surface Temperature. *Ind. Eng. Chem. Res.* **2014**, *53* (17), 7233−7246.
(50) Zbogar, A.; Frandsen, F. J.; Jensen, P. A.; Glarborg, P. Heat transfer in ash deposits: A modelling tool-box. *Prog. Energy Combust. Sci.* **2005**, *31* (5−6), 371−421.

DOI: 10.1021/acs.energyfuels.8b04199
Energy Fuels XXXX, XXX, XXX−XXX